Electron-impact ionization of Al^{2+}

Di Wu, S. D. Loch, M. S. Pindzola, and C. P. Ballance
Department of Physics, Auburn University, Auburn, Alabama 36849, USA
(Received 12 August 2011; published 25 January 2012)

We report on a nonperturbative R-matrix with PseudoStates (RMPS) calculation for the electron-impact ionization cross section of the ground state of Al^{2+}. We include both the direct ionization of the $3s$ and $2p$ subshells and the indirect ionization from the $2p$ subshell. This calculation, thus, includes extra decay channels for the indirect-ionization process not included in previous RMPS calculations. This lowers the total-ionization cross section, resulting in closer agreement with the most recent experimental measurements. This calculation also shows better agreement with the position and height of the resonant-excitation double autoionization features seen in the experiment.

DOI: 10.1103/PhysRevA.85.012711 PACS number(s): 34.80.Dp

I. INTRODUCTION

Electron-impact single ionization provides the dominant ionization mechanism for the majority of laboratory and astrophysical plasmas. Aluminum is of current interest for the Madison symmetric torus [1], which has aluminum vessel walls. Modeling the impurity transport of the Al ions into the plasma core requires accurate ionization and recombination rates for each ion stage of Al. In this paper, we focus on resolving discrepancies between the currently available theoretical cross-section data and the experimental measurements of the electron-impact single ionization of Al^{2+}.

Ionization of Al^{2+} has been studied previously both experimentally and theoretically. Al^{2+} cross sections were initially measured by Crandall *et al.* [2]. The direct ionization for this ion was calculated using the distorted-wave (DW) method by Younger [3], and DW data for the excitation-autoionization of the $2p$ subshell were calculated by Griffin *et al.* [4]. The total DW cross sections were significantly higher than the experimental measurements as one might expect for a doubly ionized system. Badnell *et al.* [5] then presented results from three nonperturbative calculations of the $3s$ ionization, using the R-matrix with PseudoStates (RMPS), the Time-Dependent Close-Coupling (TDCC), and the Convergent Close-Coupling (CCC) methods. These were found to be in reasonable agreement with each other, about 30% higher than the measurements of Crandall *et al.* [2] and significantly lower than the DW cross sections. Thomason and Peart [6] then measured the ionization cross section with results that were in excellent agreement with the nonperturbative results of Badnell *et al.* [5] at energies where the $3s$ direct ionization dominates and higher than the previous measurements of Crandall *et al.* [2]. Thomason and Peart also measured the cross section at a fine-energy resolution to map out the indirect-ionization contributions due to excitation of the $2p$ subshell. They found that configuration-average DW (CADW) calculations of the indirect contribution were much larger than their measured values. The two-state close-coupling calculations of Henry and Msezane [7] were closer to their measurements but were still higher than the experimental values. Teng [8] then performed RMPS calculations for the direct ionization of the $3s$ subshell and for the indirect ionization of the $2p$ subshell. Teng [8] used scaled DW cross sections for the $2p$ direct ionization. These theoretical results matched the shape of the indirect contributions, including features that corresponded to resonant-excitation double autoionization but were still higher than the measured values. Explaining the experimental cross sections for Al^{2+} above 80 eV is still an open question and is the subject of this paper.

In the next section, we describe the theoretical methods used in this paper. Section III then describes our results, and in Sec. IV, we summarize the work.

II. THEORY

The main contributions to the electron-impact single-ionization cross section are from direct ionization,

$$e^- + Al^{2+} \rightarrow Al^{3+} + e^- + e^-, \tag{1}$$

and excitation autoionization,

$$e^- + Al^{2+} \rightarrow (Al^{2+})^* + e^- \rightarrow Al^{3+} + e^- + e^-. \tag{2}$$

$(Al^{2+})^*$ represents an excited state of the ion, and for the process of excitation autoionization, there also is the possibility of radiative stabilization occurring before the excited ion can autoionize. Thus, autoionizing configurations are associated with an Auger yield, giving the fraction of electrons that autoionize from such a configuration. For Al^{2+}, the Auger rates are much larger than the radiative rates, and it is a reasonable approximation to assume that the Auger yield is 100%. The excitation autoionization for Al^{2+} proceeds predominantly via a $2p$ core excitation and contributes a non-negligible amount to the total cross section.

It is also possible for the excitation in the first step of Eq. (2) to proceed via a dielectronic capture [into $(Al^{+})^*$], which subsequently autoionizes to the excited state $(Al^{2+})^*$ in Eq. (2). Then, this state can autoionize as indicated in the rest of Eq. (2). These resonant features on the excitation cross sections are known as resonant-excitation double autoionization (REDA) features. Alternatively, the state formed from the dielectronic capture can undergo an auto-double ionization, known as resonant-excitation auto-double ionization (READI). One of the unique aspects of the high-resolution scan performed by Thomason and Peart [6] was that such resonant features were observed in the total cross sections. Teng [8] showed theoretically that REDA did contribute a significant fraction

to the indirect ionization and also showed that READI made a small contribution for this ion.

Thus, the total cross section, considering both direct and indirect processes is

$$\sigma_{\text{total}} = \sum_i \sigma_{\text{direct}} + \sum_j \sigma_{\text{indirect}}, \tag{3}$$

where the sum i is over the direct-ionization channels and the sum j is over the inner subshell electrons, which can be excited (both directly and via a resonance state), leading to an autoionizing configuration.

A. Configuration-Average Distorted-Wave Method

The direct-ionization process can be evaluated using the CADW method [9], representing the transition,

$$(nl)^w k_i l_i \rightarrow (nl)^{w-1} k_e l_e k_f l_f, \tag{4}$$

where w is the occupation number of the initial subshell being ionized, $k_i l_i$ are the quantum numbers of the incident electron, while $k_e l_e$ and $k_f l_f$ are the quantum numbers for the ejected and final continuum electrons, respectively. The configuration-average direct cross section is given by

$$\sigma = \frac{32\omega}{k_i^3} \int_0^{E/2} \frac{d\left(k_e^2/2\right)}{k_e k_f} \sum_{l_i,l_e,l_f} (2l_i+1)(2l_e+1) \times (2l_f+1) P(l_i,l_e,l_f,k_i,k_e,k_f), \tag{5}$$

where $E = \frac{1}{2}(k_e^2 + k_f^2)$ and P is the first-order scattering probability, which previously was described in more detail [9].

There are commonly two different approximations made for the scattering potential that the incident, scattered, and ejected electrons experience. In what is referred to as the DW incident and scattered (DWIS)(N) method, the incident and scattered electrons are evaluated in a V^N potential, with the ejected continuum electron calculated in a V^{N-1} potential, where N is the number of electrons in the initial target. Alternatively, one can calculate the incident, scattered, and ejected electrons in a V^{N-1} potential, labeled as DWIS($N-1$). We use the DWIS($N-1$) method throughout this paper.

The CADW method also can be used to calculate the excitation-autoionization contribution [9]. In the configuration-average approach, the excitation process is represented by

$$(n_1 l_1)^{w_1+1} (n_2 l_2)^{w_2-1} k_i l_i \rightarrow (n_1 l_1)^{w_1} (n_2 l_2)^{w_2} k_f l_f, \tag{6}$$

where $n_1 l_1$ and $n_2 l_2$ are quantum numbers of the bound electrons and $k_i l_i$ and $k_f l_f$ are quantum numbers of the initial and final continuum electrons, respectively. The configuration-average excitation cross section is given by

$$\sigma_{\text{exc}} = \frac{8\pi}{k_i^3 k_f}(w_1+1)(4l_2+3-w_2) \times \sum_{l_i,l_f} (2l_i+1)(2l_f+1) P(l_i,l_f,k_i,k_f), \tag{7}$$

where P is the first-order scattering probability [9]. While we calculate DW cross sections for the direct ionization and excitation autoionization of Al^{2+}, we do not evaluate any REDA or READI contributions. We note that, it has already been shown that DW ionization cross sections overestimate the total cross section [5]. Here, we include the DW results as a comparison to our new R-matrix results, showing how much a perturbative method overestimates the cross section.

B. R-Matrix with PseudoStates Method

We use the RMPS method [10,11] to calculate ionization cross sections for Al^{2+}. Our codes are based upon significantly modified versions of the serial RMATRIX I programs [12]. The basis used to represent the $(N+1)$-electron continuum is made orthogonal to the pseudo-orbitals using a method developed by Gorczyca and Badnell [11]. We use Laguerre polynomials to represent the pseudostates,

$$P_{nl}(r) = N_{nl}(\lambda_l Zr)^{l+1} e^{-\lambda_l Zr/2} L_{n+1}^{2l+1}(\lambda_l Zr). \tag{8}$$

Here, $Z = z+1$, where z is the residual charge on the ion, $L_{n+1}^{2l+1}(\lambda_l Zr)$ represents the Laguerre polynomial, N_{nl} is a normalization constant, n and l are the quantum numbers, and λ_l is the orbital scaling parameter.

The codes have undergone significant parallelization to optimize their use on supercomputers [13,14]. Our RMPS calculations were large in size, taking advantage of a recent development in the codes. With each $(N+1)$ electron-scattering symmetry being carried out concurrently, within each symmetry, we group N-electron terms of the same $LS\pi$ together and simultaneously calculate the continuum-continuum $(N+1)$-electron Hamiltonian blocks for each grouping [15].

R-matrix theory dictates that the configuration space describing the scattering processes is split into two regions. In the inner region, which encompasses the N-electron target, the total wave function for a given $LS\pi$ symmetry is expanded in basis states given by

$$\Psi_k^{N+1} = A \sum_{i,j} a_{ijk} \psi_i^{N+1} \frac{u_{ij}(r_{N+1})}{r_{N+1}} + \sum_i b_{ik} \chi_i^{N+1}, \tag{9}$$

where A is an antisymmetrization operator, ψ_i^{N+1} are channel functions obtained by coupling N-electron target states with the angular and spin functions of the scattered electron, $u_{ij}(r)$ are radial continuum basis functions, and χ_i^{N+1} are bound functions that ensure completeness of the total wave function. The coefficients a_{ijk} and b_{ik} are determined by diagonalization of the total $(N+1)$-electron Hamiltonian. The availability of modern supercomputing architectures permits the concurrent parallel diagonalization of every Hamiltonian utilizing ScaLAPACK libraries [16]. The resulting eigenvalues and eigenvectors are subsequently used in the formation of the R-matrix.

In the outer region, the total wave function for a given $LS\pi$ symmetry is expanded in basis states given by

$$\Psi_k^{N+1} = \sum_i \psi_i^{N+1} \frac{v_i(r_{N+1})}{r_{N+1}}. \tag{10}$$

For RMPS ionization calculations, the ionization cross section is derived from the sum of excitation cross sections from the ground-state term to those pseudostates lying above the respective ionization limit, where the ionization potential (72.884 eV) is obtained from the National Institute of

Standards and Technology (NIST) [17] database. That is, the NIST ionization potential is used to determine the first R-matrix pseudostate that is in the continuum. The R-matrix cross section is given by

$$\sigma(i,j) = \frac{\pi}{k^2} \sum_{LS\pi l_i l_j} \frac{(2L+1)(2S+1)}{2(2L_i+1)(2S_i+1)} |S^{LS\pi}|^2, \quad (11)$$

where i is the initial state, j is the final state, and $S_i L_i$ are the total spin and total orbital angular momentum of the initial state. The sum is over the partial waves, and $S^{LS\pi}$ is the S matrix for an $LS\pi$ symmetry. We note that our total RMPS cross sections contain direct ionization, excitation-autoionization, REDA, and READI contributions.

III. RESULTS

Previously, Al^{2+} had been studied extensively, and while nonperturbative calculations have shown good agreement with the lower-energy measurements of Thomason and Peart [6], there is still significant disagreement in the region where indirect ionization due to the $2p$ subshell contributes to the total cross section. We used the multiconfiguration Breit-Pauli structure code AUTOSTRUCTURE [18] to generate our radial orbitals in a Thomas-Fermi Amaldi-Dirac potential. To investigate this, we set up three RMPS calculations. The first one calculated just the $3s$ direct ionization using a set of $2p^6nl$ configurations where $3s < nl < 14h$ ($0 \leqslant l \leqslant h$). We used spectroscopic orbitals up to the $5g$ subshell and pseudostates for the higher subshells. In our AUTOSTRUCTURE calculation, we used the orbital scaling parameters for the pseudo-orbitals to achieve an even spread of the pseudostates across the ionization potential. We used the following scaling parameters for our radial pseudostates: $\bar{n}s = 0.99$, $\bar{n}p = 0.92$, $\bar{n}d = 0.82$, $\bar{n}f = 0.84$, $\bar{n}g = 0.9$, and $\bar{n}h = 1.12$. These are the λ_l's in Eq. (8). We refer to this calculation as $RMPS_{3s}$. Thus, this is a similar calculation to the RMPS calculation of Badnell *et al.* [5], although much larger in size.

Our second RMPS calculation for this ion used the $2p^5 3snl$ configurations where $3s < nl < 13g$ ($0 \leqslant l \leqslant g$). We used spectroscopic orbitals up to the $3d$ subshell, pseudostates for the higher subshells, and orbital scaling parameters for the s and p pseudo-orbitals to evenly distribute their terms over the ionization potential. We note that we chose hydrogenic scaling parameters for the remaining d, f, and g pseudo-orbitals, otherwise the size of the R-matrix box would be too large. We used $\bar{n}s = 1.08$ and $\bar{n}p = 1.02$. We refer to this calculation as $RMPS_{2p}$. While this calculation has both direct ionization of the $2p$ and excitation autoionization of the $2p$ subshell, many Auger channels for the resonances attached to the excited configurations are missing, meaning that the heights of these resonant features may be artificially large. These channels were also missing from the calculation of Teng [8], and in that paper, it was postulated that this was the reason that the RMPS results were higher than the experiment of Thomason and Peart [6].

Thus, our third RMPS calculation included the $2p^6nl$ and $2p^5 3snl$ configurations, where $3s < nl < 14g$. We used spectroscopic orbitals up to $3d$ and pseudostates for the higher subshells and used orbital scaling parameters to evenly distribute the s and p pseudo-orbitals over the ionization potential ($\bar{n}s = 1.03$, $\bar{n}s = 1.04$). Thus, this calculation includes both the direct ionization of the $3s$ and $2p$ subshells and the indirect processes associated with the $2p$ subshell. Due to the inclusion of the $2p^6nl$ pseudostates in the calculation, we allow for Auger decay of the REDA and READI resonant features in the $2p$ indirect-ionization cross section. We also shift the following term energies in the prediagonalization of the $(N+1)$ Hamiltonian of the RMPS calculation to match the NIST values: $2p^5 3s^2(^2P)$, $2p^5 3s 3p(^4D, {}^4P, {}^2D, {}^2P)$, $2p^5 3p^2(^2P^o, {}^4D^o)$, and $2p^5 3s 3d(^4P^o, {}^4F^o, {}^4D^o, {}^2D^o, {}^2P^o)$. We refer to this calculation as $RMPS_{3s2p}$.

Table I shows the energies of the terms that are expected to provide the dominant contribution to excitation autoionization and their corresponding NIST energies. Figure 1 shows the results for the two experimental measurements along with previous theoretical results for the direct ionization of the $3s$ subshell. We also show the results from our $RMPS_{3s}$ calculation. We note that our $RMPS_{3s}$ results are in good agreement with the previous nonperturbative calculations (RMPS and TDCC) of Badnell *et al.* [5], and are in good agreement with the experimental measurements of Thomason and Peart [6] at energies below which the $2p$ subshell starts to contribute, about 75 eV. This again supports the previous conclusion that the measurements of Crandall *et al.* [2] are spuriously low. DW results already have been shown to be

TABLE I. Term energies from AUTOSTRUCTURE model $RMPS_{3s2p}$ and corresponding NIST energies.

Configuration	AUTOSTRUCTURE result (Ry)	NIST value (Ry)	Difference (%)
$2p^5 3s^2(^2P^o)$	5.457	5.3734	1.55
$2p^5 3s 3p(^4S)$	5.720	5.6978	0.38
$2p^5 3s 3p(^4D)$	5.793	5.7743	0.33
$2p^5 3s 3p(^4P)$	5.840	5.8129	0.47
$2p^5 3s 3p(^2D)$	5.860	5.8390	0.36
$2p^5 3s 3p(^2P)$	5.877	5.8540	0.39
$2p^5 3s 3d(^4P^o)$	6.566	6.5241	0.65
$2p^5 3s 3d(^4F^o)$	6.583	6.5274	0.86
$2p^5 3s 3d(^4D^o)$	6.612	6.5640	0.73
$2p^5 3s 3d(^2D^o)$	6.645	6.6024	0.65
$2p^5 3s 3d(^2P^o)$	6.654	6.6205	0.51

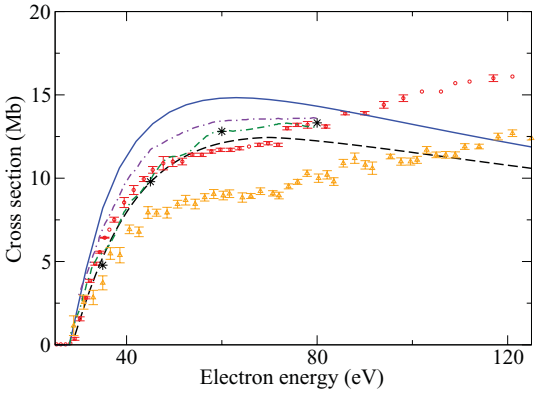

FIG. 1. (Color online) Electron-impact ionization cross section for Al^{2+}. The dashed curve (black) shows the $RMPS_{3s}$ calculations. The solid curve (blue) shows the DW results for the $3s$ ionization only. The up triangles (yellow) show the experimental measurements of Crandall *et al.* [2], and the circles (red) show the experimental measurements of Thomason and Peart [6]. Also shown are the RMPS [double-dashed-dotted line (green)], TDCC [stars (black)], and CCC [dashed-dotted line (purple)] results from Badnell *et al.* [5].

higher than both the experimental measurements and the nonperturbative theoretical results [5].

Figure 2 shows our $RMPS_{2p}$ results. For clarity in the plot, we only show the experimental results of Thomason and Peart [6]. The DW results for the $2p$ ionization (which includes no REDA or READI contributions) are about 30% higher than the $RMPS_{2p}$ cross section. Our total RMPS cross section is a sum of the $RMPS_{3s}$ and $RMPS_{2p}$ cross sections and is clearly higher by about 15%–20% than the experimental measurements, showing very large REDA features above about 75 eV. This is similar to the findings of Teng [8] who pointed out that, without the Auger decay channels for the REDA features in a calculation of the $2p$ contribution, the resonances would be spuriously high.

Figure 3 shows the results from our $RMPS_{3s2p}$ calculation. The heights of the resonance features are much reduced,

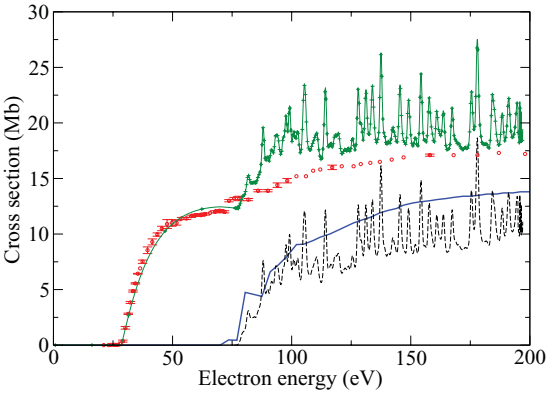

FIG. 2. (Color online) Electron-impact ionization cross section for Al^{2+}. The dashed curve (black) shows the $RMPS_{2p}$ results. The solid curve (blue) shows the DW results for the $2p$ ionization only (direct ionization + excitation autoionization). The circles (red) show the experimental measurements of Thomason and Peart [6]. The stars (green) connected with the solid line show the $RMPS_{3s} + RMPS_{2p}$ results.

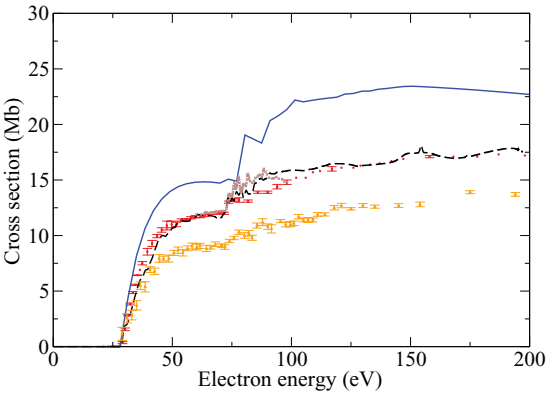

FIG. 3. (Color online) Electron-impact ionization cross section for Al^{2+}. The dashed curve (black) shows the $RMPS_{3s2p}$. The raw RMPS cross section has been convolved with a 1-eV Gaussian. The solid curve (blue) shows the DW results for the $3s$ and $2p$ ionizations. The up triangles (yellow) show the experimental measurements of Crandall *et al.* [2], and the circles (red) show the experimental measurements of Thomason and Peart [6]. The R-matrix calculation of Teng [8] is denoted by crosses (tan) and can be seen in more detail in Fig. 4.

compared with the $RMPS_{2p}$ results, and the background cross section is also reduced in height. The total cross section is now in much better agreement with the experimental measurements of Thomason and Peart [6] and is lower than the RMPS results of Teng [8]. We also note that the contribution due to the $3s$ near 60 eV is also reduced slightly and is in better agreement with the experiment. We show our RMPS results convolved with a 1 eV Gaussian as previously determined by Teng [8] to best match the experimental resolution. The DW results are up to 35% higher than the experimental measurements. We note that we have excellent agreement across almost the whole energy range of the experiment, with some small discrepancies remaining from 80 to 100 eV.

In Fig. 4, we show results for the region of 70–110 eV, comparing our $RMPS_{3s2p}$ cross section with the experiment of Thomason and Peart [6] and the RMPS results of Teng [8].

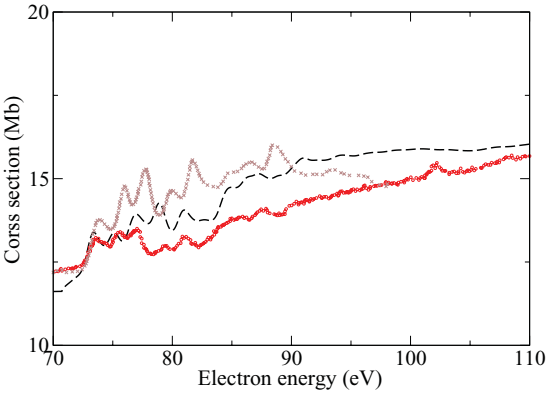

FIG. 4. (Color online) Electron-impact ionization cross section for Al^{2+}. The dashed curve (black) shows the $RMPS_{3s2p}$ results. The raw RMPS cross section has been convolved with a 1 eV Gaussian. The circles (red) show the fine-energy scan experimental measurements of Thomason and Peart [6]. The crosses (tan) show the R-matrix calculation of Teng [8].

In the 70–90 eV region, we have much better agreement with the resonance position and heights than the previous results of Teng [8]. Above about 75 eV, we are still about 15% higher than the experimental measurements, with the discrepancy being perhaps due to sensitivity in the cross section to the resonance positions of these features. We note that the level of discrepancy that remains is not sufficient to significantly affect the ionization balance results that would be produced using the data.

IV. CONCLUSIONS

We have reported on RMPS results for the single ionization of Al^{2+}. When both the $3s$ and $2p$ ionization channels are included in a single calculation, much better agreement is found with the experimental measurements of Thomason and Peart [6]. Maxwellian rate coefficients have been made from the cross sections and will be made available on the CFADC [19] and OPEN-ADAS [20].

[1] S. T. A. Kumar, D. J. D. Hartog, R. M. Magee, G. Fiksel, and D. Craig, Plasma Phys. Controlled Fusion **53**, 032001 (2011).
[2] D. H. Crandall, R. A. Phaneuf, R. A. Falk, D. S. Belic, and G. H. Dunn, Phys. Rev. A **25**, 143 (1982).
[3] S. M. Younger, Phys. Rev. A **24**, 1272 (1981).
[4] D. C. Griffin, C. Bottcher, and M. S. Pindzola, Phys. Rev. A **25**, 154 (1982).
[5] N. R. Badnell, M. S. Pindzola, I. Bray, and D. C. Griffin, J. Phys. B **31**, 911 (1998).
[6] J. W. G. Thomason and B. Peart, J. Phys. B **31**, L201 (1998).
[7] R. J. W. Henry and A. Z. Msezane, Phys. Rev. A **26**, 2545 (1982).
[8] H. Teng, J. Phys. B **33**, L553 (2000).
[9] M. S. Pindzola, D. C. Griffin, and C. Bottcher, in *Atomic Processes in Electron-Ion and Ion-Ion Collisions*, edited by F. B. Plenum, NATO Advanced Study Institute, Series B: Physics (Plenum, New York, 1986), Vol. 145.
[10] K. Bartschat, E. Hudson, M. Scott, P. Burke, and V. Burke, J. Phys. B **29**, 115 (1996).
[11] T. W. Gorczyca and N. R. Badnell, J. Phys. B **30**, 3897 (1997).
[12] K. A. Berrington, W. B. Eissner, and P. H. Norrington, Comput. Phys. Commun. **92**, 290 (1995).
[13] D. M. Mitnik, D. C. Griffin, C. P. Ballance, and N. R. Badnell, J. Phys. B **36**, 717 (2003).
[14] C. P. Ballance and D. C. Griffin, J. Phys. B **37**, 2943 (2004).
[15] C. P. Ballance, J. A. Ludlow, M. S. Pindzola, and S. D. Loch, J. Phys. B **42**, 175202 (2009).
[16] L. S. Blackford *et al.*, *ScaLAPACK Users' Guide* (SIAM, Philadelphia, 1997).
[17] NIST ASD Team, *Nist Atomic Spectra Database* [http://physics.nist.gov/asd3].
[18] N. R. Badnell, J. Phys. B **30**, 1 (1997).
[19] [http://www-cfadc.phy.ornl.gov/data_and_codes/home.html].
[20] [http://open.adas.ac.uk/].